Implications of recently derived thermodynamic data and specific ionic interaction theory parameters for $(Mg/Ca)_nUO_2(CO_3)_3^{(4-2n)-}$ complexes on the predominance of the Mg^{2+}–Ca^{2+}–UO_2^{2+}–OH^-–CO_3^{2-} systems, and application to natural and legacy-mine waters.

Chengming Shang,[a,†] Nathalie Coreau,[b] Nathalie Macé,[b] Michael Descostes,[c,d] and Pascal E. Reiller[a,*]

a Université Paris-Saclay, CEA, Service d'Études Analytiques et de Réactivité des Surfaces (SEARS), F-91191 Gif-sur-Yvette CEDEX, France.

b Université Paris-Saclay, CEA, Service d'Études du Comportement des Radionucléïdes (SECR), F-91191 Gif-sur-Yvette CEDEX, France.

c ORANO Mining, Environmental R&D Department, 125 Avenue de Paris, 92330, Châtillon, France.

d PSL University/Mines ParisTech, Centre de Géosciences, 35 rue Saint-Honoré, 77305, Fontainebleau, France.

Corresponding author's e-mail: pascal.reiller@cea.fr.

† present address: Karlsruhe Institute of Technology, Institute for Nuclear Waste Disposal, P.O. Box 3640, 76021, Karlsruhe, Germany

Supplementary Figures

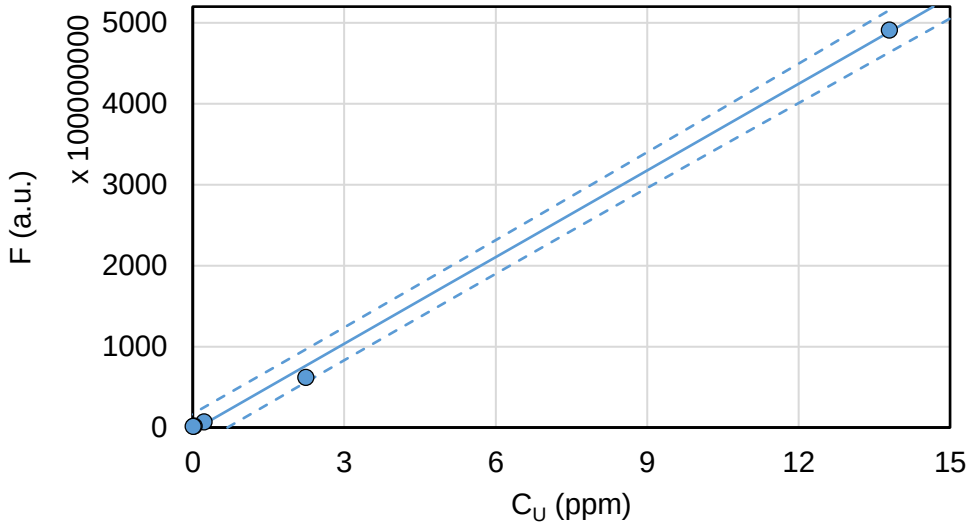

a = (3.57 ± 0.08) 10^{10}	b = (-3.67 ± 4.84) 10^{9}
r^2 = 0.9986	Sx/y = 9.243 10^{9}
DoF = 3	
$\bar{y}$ = 1.125 10^{11}	SSR(x) = 142.409

Figure S1. Calibration of the TRLFS analysis of uranium in 5% .wt H_3PO_4.

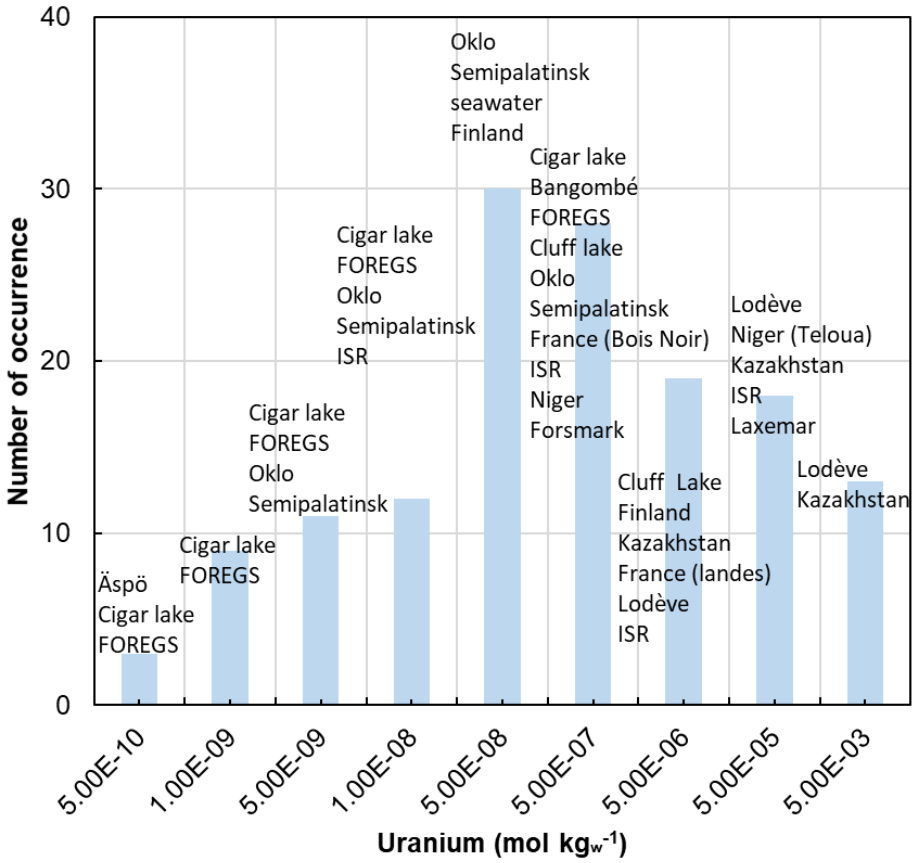

Figure S2. Frequency distribution of the uranium concentration from literature.

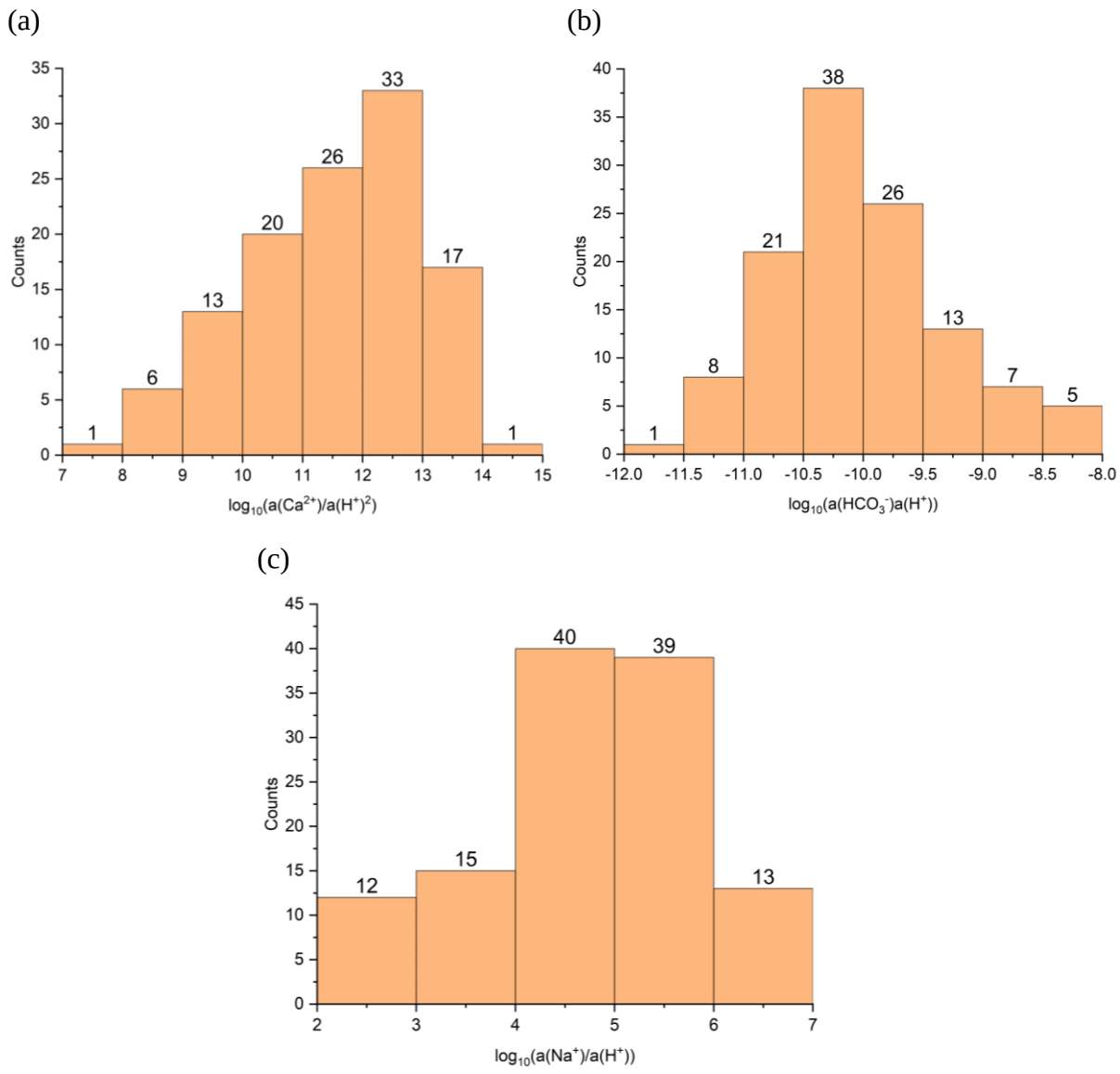

Figure S3. Frequency distributions of the (a) $\log_{10}(a(Ca^{2+})/a(H^{+})^{2})$, (b) $\log_{10}(a(HCO_3^{-})\, a(H^{+}))$, and (c) $\log_{10}(a(Na^{+})/a(H^{+}))$ parameters for the selected sample solutions.

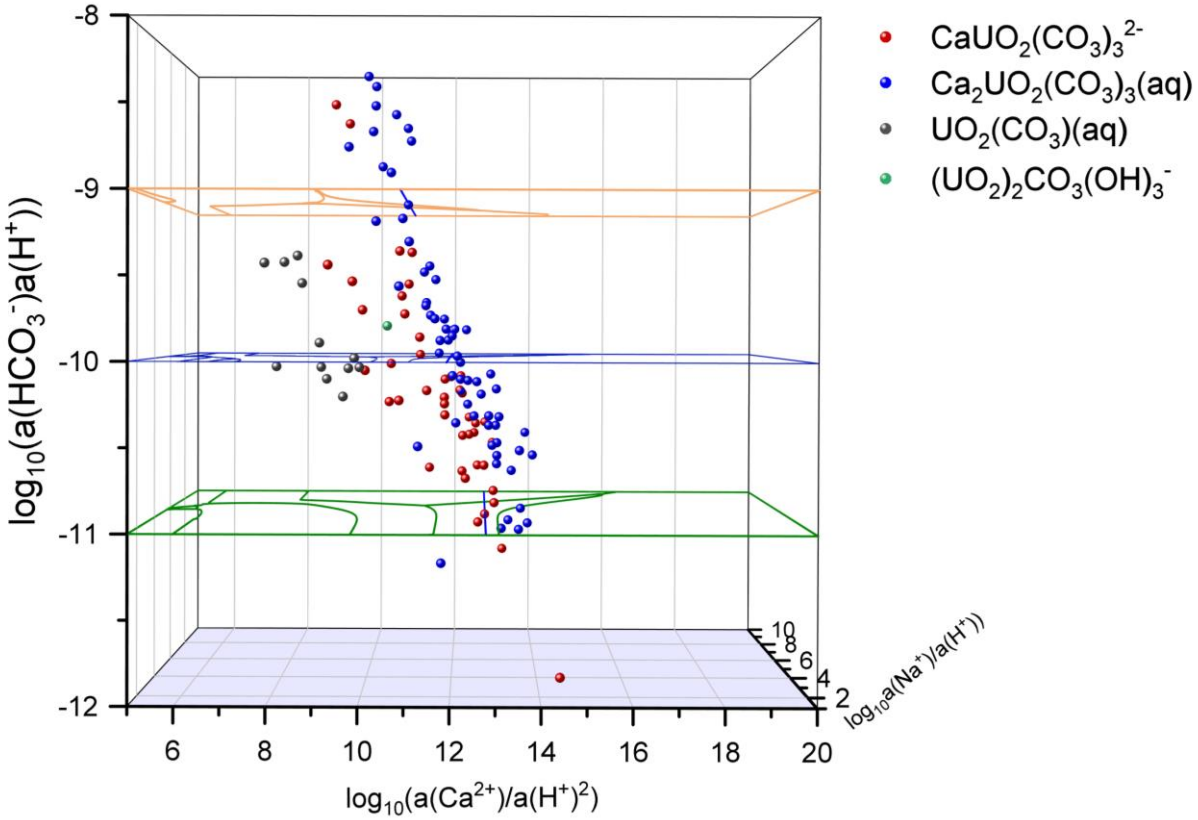

Figure S4. Repartition of the major species in the speciation calculations of the selected water compositions in a $\log_{10}(a(Ca^{2+})/a(H^+)^2)$–$\log_{10}(a(Na^+)/a(H^+))$–$\log_{10}(a(HCO_3^-)\ a(H^+))$ diagram; the values of $\log_{10}(a(HCO_3^-)\ a(H^+))$ were respectively fixed to -11, -10, -9 to deduce the $\log_{10}(a(Ca^{2+})/a(H^+)^2)$–$\log_{10}(a(Na^+)/a(H^+))$ predominance diagrams.

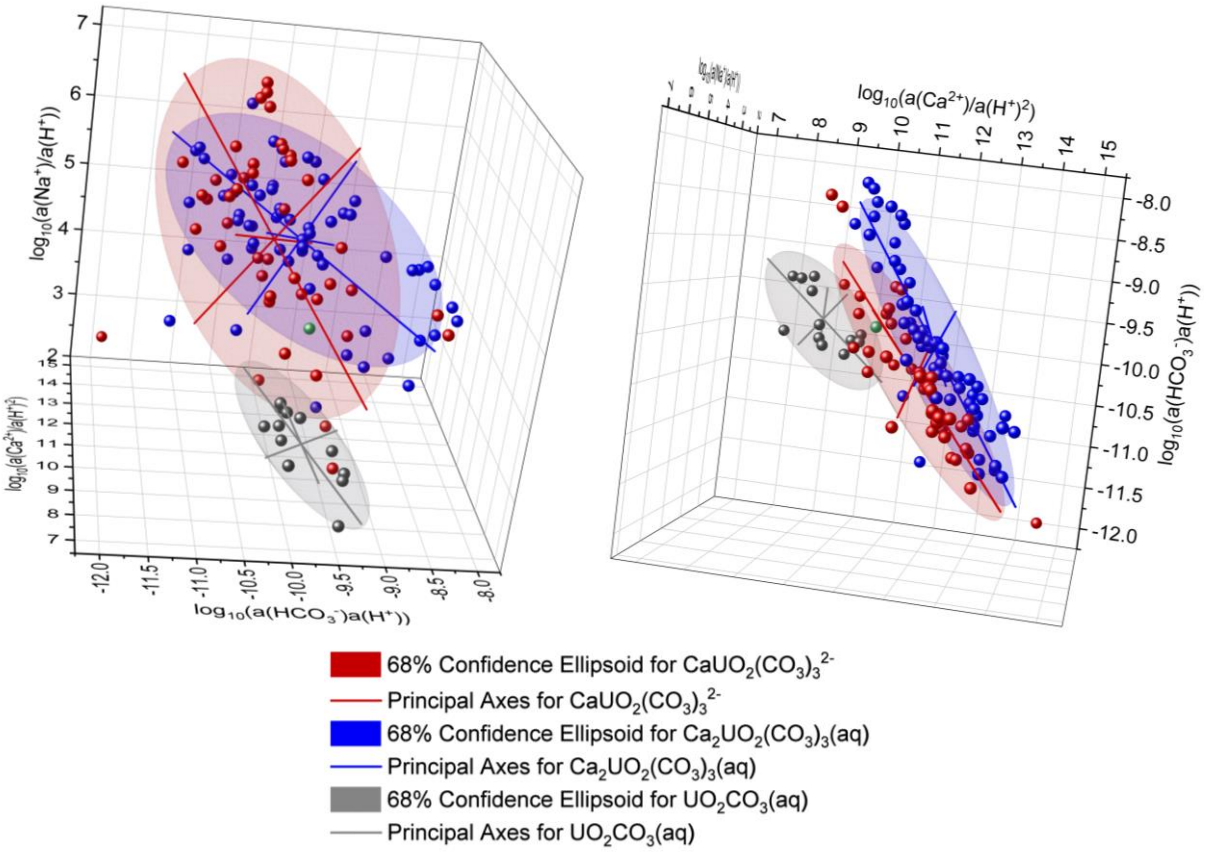

Figure S5. Ellipsoidal predominance regions of UO_2CO_3(aq) (grey), $CaUO_2(CO_3)_3^{2-}$ (red), and $Ca_2UO_2(CO_3)_3$(aq) (blue) in $\log_{10}(a(Ca^{2+})/a(H^+)^2)$–$\log_{10}(a(Na^+)/a(H^+))$–$\log_{10}(a(HCO_3^-)\,a(H^+))$ space determined from the sample point-clouds with the interval confidence of 68% from Figure 9 of the main text, seen from two other angles.

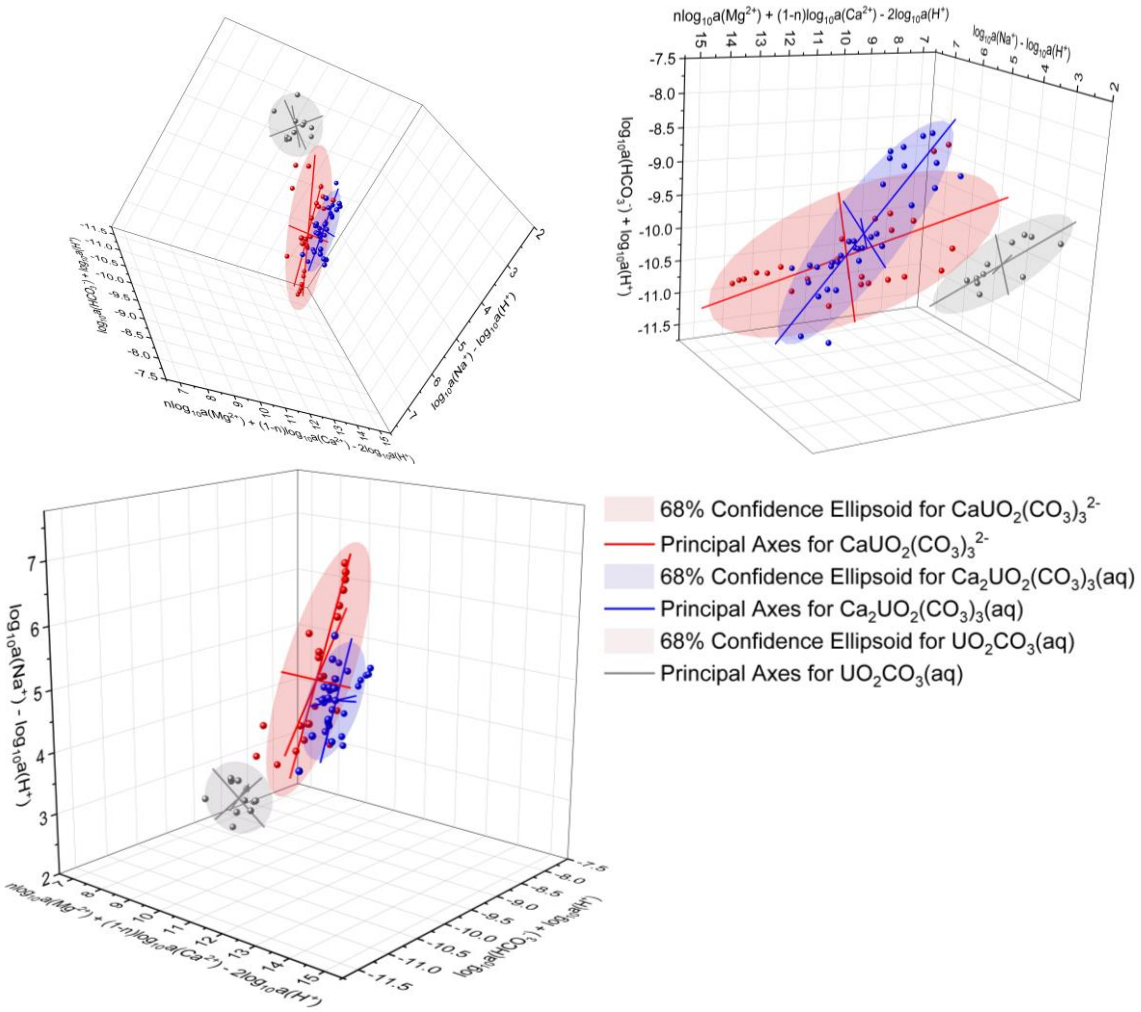

Figure S6. Ellipsoidal predominance regions of $UO_2CO_3(aq)$ (grey), $CaUO_2(CO_3)_3^{2-}$ (red), and $Ca_2UO_2(CO_3)_3(aq)$ (blue) in $\log_{10}(a(Mg^{2+})^n\, a(Ca^{2+})^{(1-n)}/a(H^+ {+}^+H)^2)$–$\log_{10}(a(Na^+)/a(H^+))$–$\log_{10}(a(HCO_3^-)\, a(H^+))$ space determined from the sample point-clouds with the interval confidence of 68%, seen from three different angles.

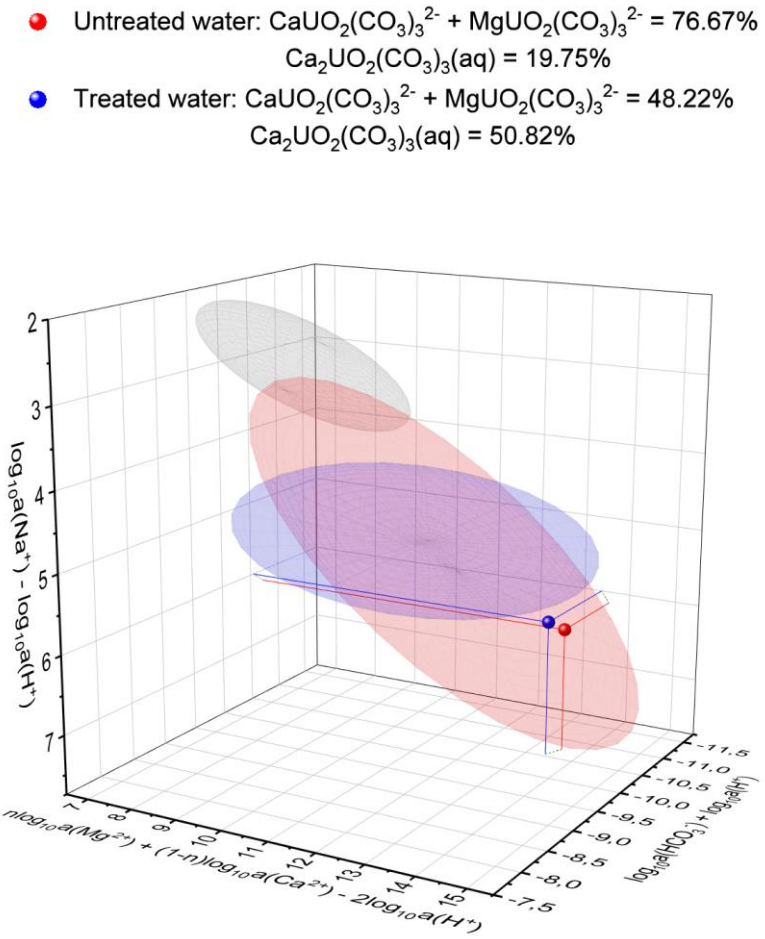

Figure S7. Position of the two Lodève water samples in a $\log_{10}(a(Mg^{2+})^n\, a(Ca^{2+})^{(1-n)}/a(H^+ + {}^+H)^2) – \log_{10}(a(Na^+)/a(H^+)) – \log_{10}(a(HCO_3^-)\, a(H^+))$ diagram. Ellipsoidal predominance regions of UO_2CO_3(aq) (grey), $CaUO_2(CO_3)_3^{2-}$ (red), and $Ca_2UO_2(CO_3)_3$(aq) (blue) space determined from the sample point-clouds with the interval confidence of 68%.

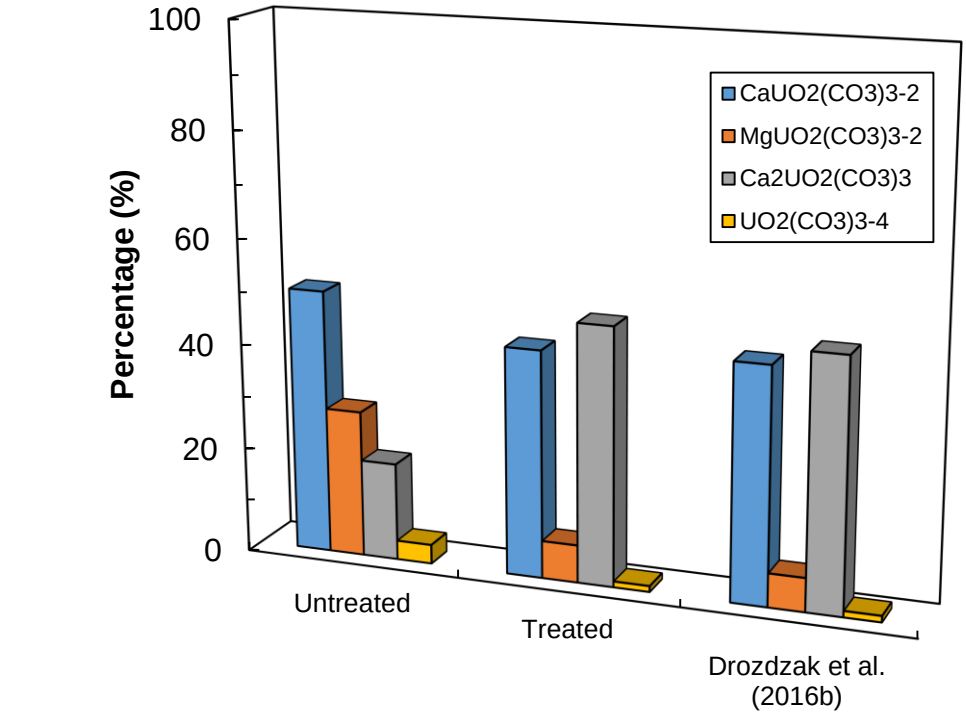

a

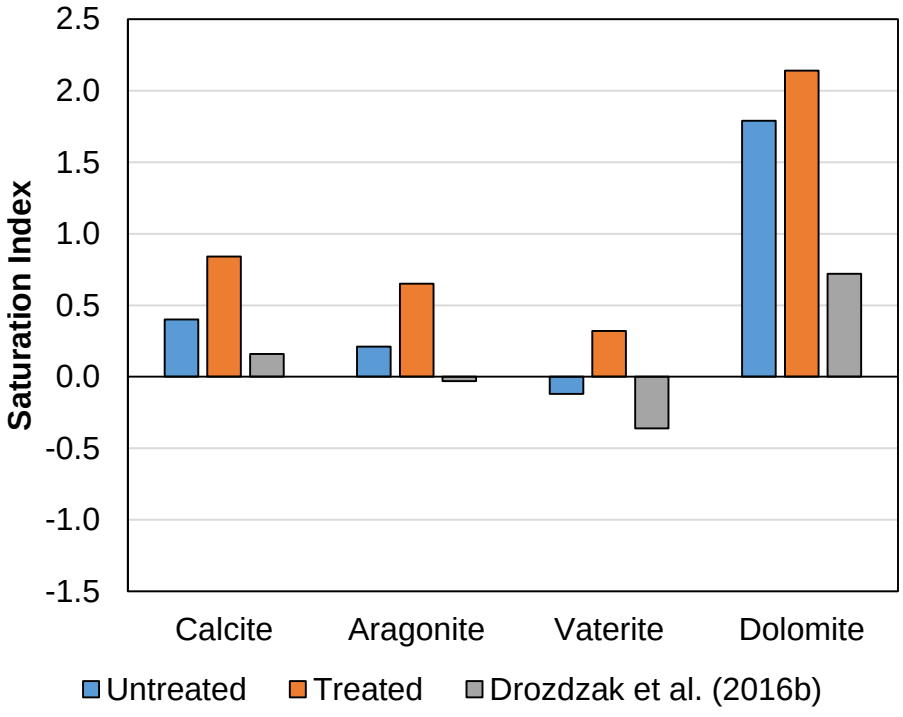

b

Figure S8. Graphical representation of the uranium speciation using SIT in Table 3 of the main text (a), and calculated saturation index of $CaCO_3$ and $MgCa(CO_3)_2$ phases (b).

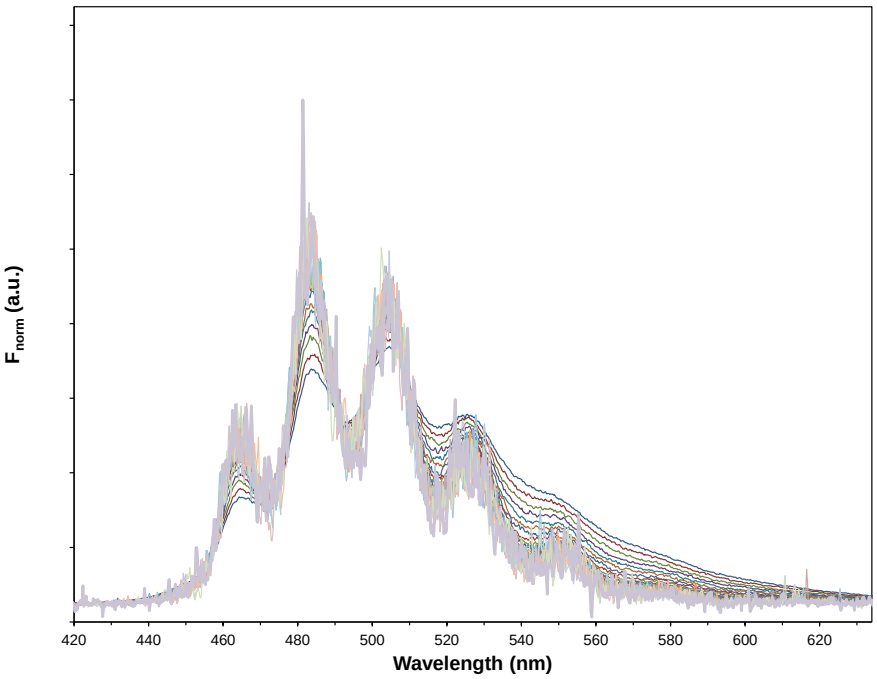

Figure S9. Normalized luminescence spectra of uranium at varying delay time for the untreated water from the site du Bosc.

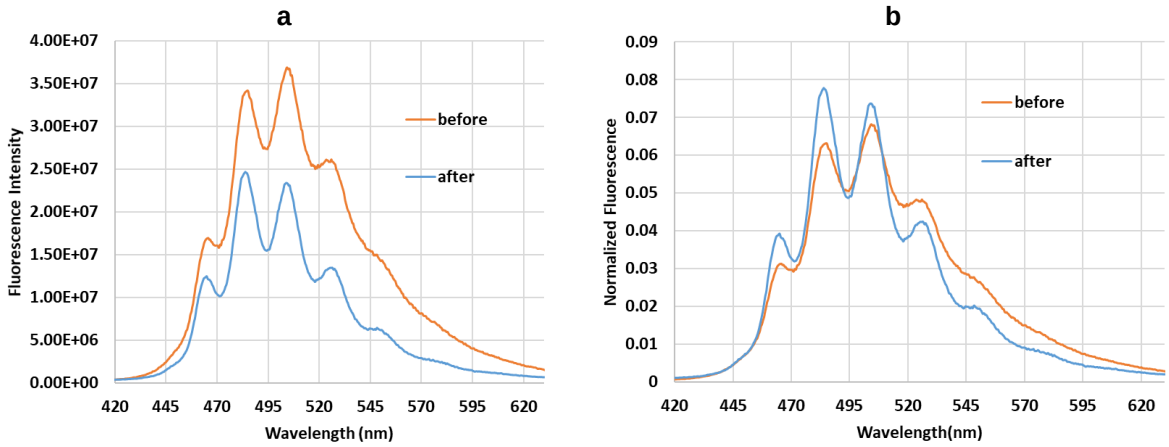

Figure S10. Comparison of (a) luminescence spectra of uranium in the untreated water sample from the site du Bosc at 25°C with delay time of D = 15 ns and gate width W = 50 ns before and after long period (≈ 5h) laser excitation at 450 nm. (b) Normalized spectra to the same area.

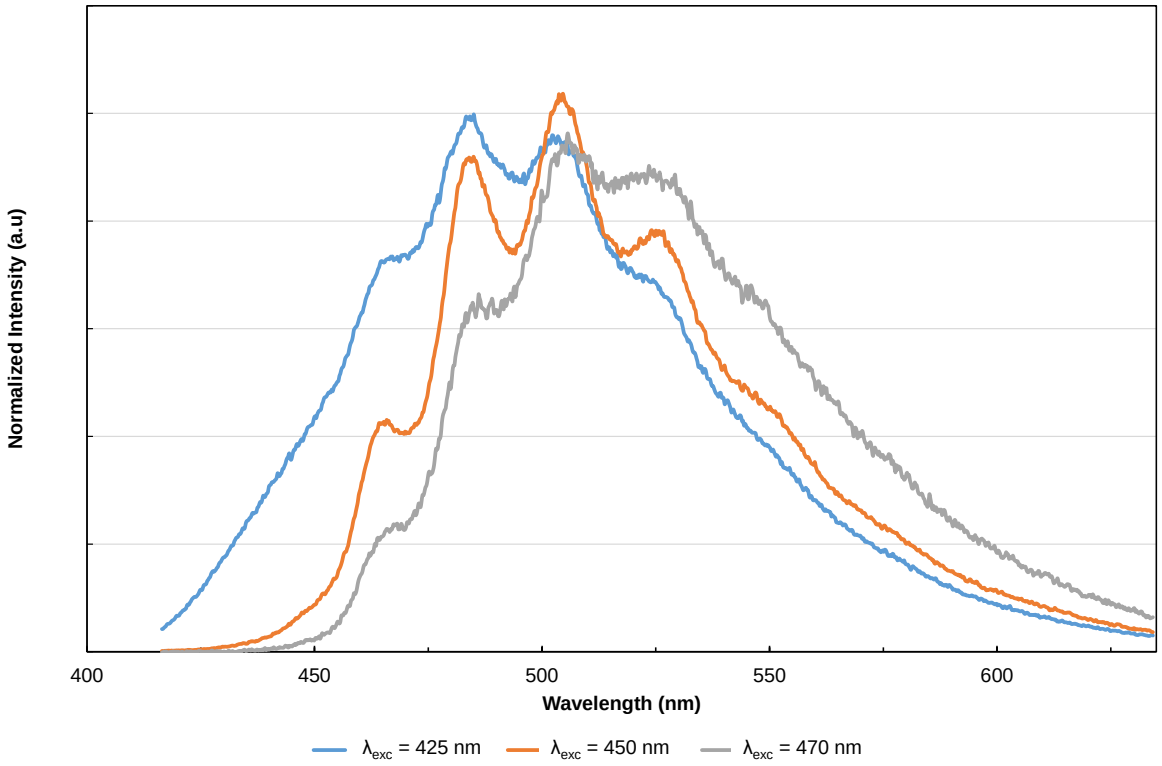

Figure S11. Comparison of fluorescence spectra normalized to the same areas of treated water from the site du Bosc at 25 °C, *D* = 20 ns, *W* = 50 ns, at varying excitation wavelength (λ_{exc}) of 425 (blue), 450 (orange), and 470 (grey) nm.

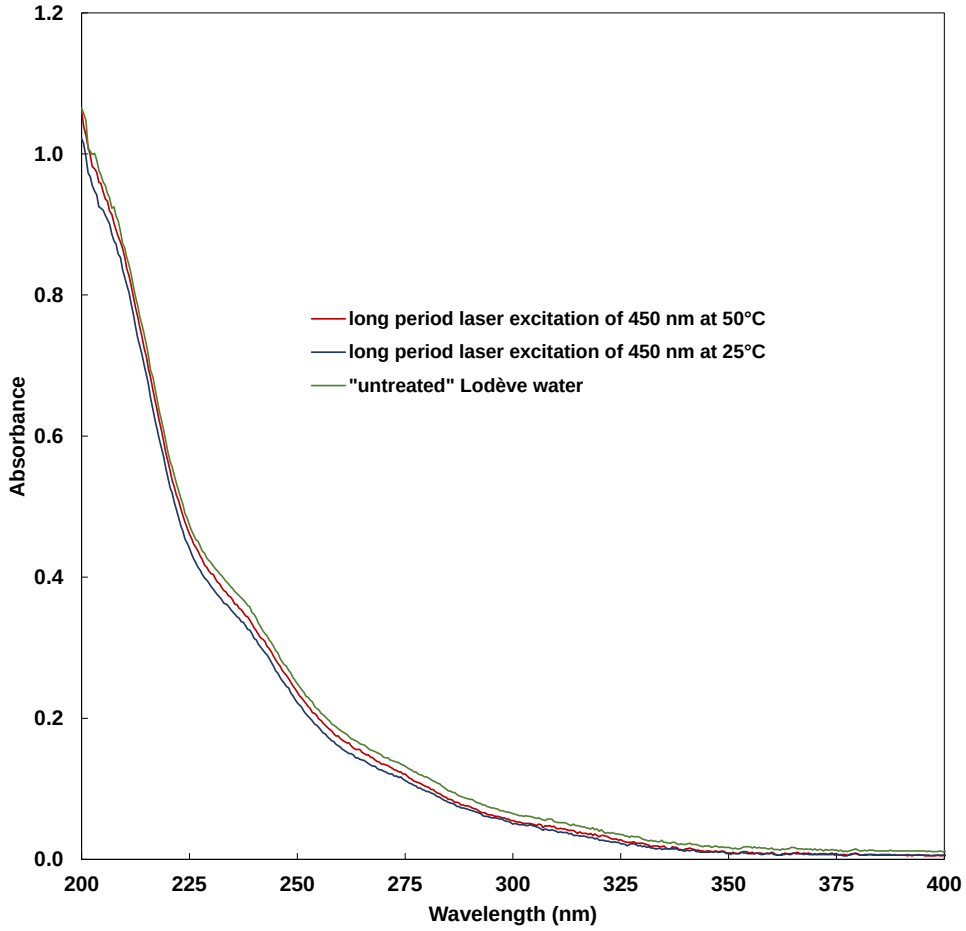

Figure S12. UV/Vis absorption of untreated water samples from the site du Bosc in the range 200 to 400 nm; green line, original water exempt from interruption of temperature and laser excitation; blue line, water sample subjected to long period (≈ 5h) laser excitation of 450 nm at 25°C; red line, water sample subjected to long period (≈ 5h) laser excitation of 450 nm at 50°C.

Supplementary Tables

Table S1. Main uranium thermodynamic data and SIT coefficients in the Thermochimie database file, or otherwise stated, used in this study.

Equilibria	$\log_{10}\beta°$	$\Delta_r H°$ kJ mol^{-1}	ε(M,NaCl) kg$_w$ mol^{-1}
$UO_2^{2+} + H_2O \rightleftarrows UO_2(OH)^+ + H^+$	-5.25	43.458	-0.003
$UO_2^{2+} + 2H_2O \rightleftarrows UO_2(OH)_2 + 2H^+$	-12.15	111.16	-
$UO_2^{2+} + 3H_2O \rightleftarrows UO_2(OH)_3^- + 3H^+$	-20.25	148.06	-0.09
$UO_2^{2+} + 4H_2O \rightleftarrows UO_2(OH)_4^{2-} + 4H^+$	-28.10	-	-
$UO_2^{2+} + CO_3^{2-} \rightleftarrows UO_2(CO_3)$	9.94	5.0	-
$UO_2^{2+} + 2CO_3^{2-} \rightleftarrows UO_2(CO_3)_2^{2-}$	16.61	18.5	-0.02
$UO_2^{2+} + 3CO_3^{2-} \rightleftarrows UO_2(CO_3)_3^{4-}$	21.84	-39.2	-0.01
$2UO_2^{2+} + CO_3^{2-} + 3\,H_2O \rightleftarrows (UO_2)_2(CO_3)(OH)_3^- + 3H^+$	-0.86	-	0
$Ca^{2+} + UO_2^{2+} + 3CO_3^{2-} \rightleftarrows CaUO_2(CO_3)_3^{2-}$	27.20[a]	-34.32[b]	0.29[a]
	27.0[c]	-	-
	27.18[d]	-	-0.02[d]
$2Ca^{2+} + UO_2^{2+} + 3CO_3^{2-} \rightleftarrows Ca_2UO_2(CO_3)_3$	30.49[a]	-40.45[b]	0.66[a]
	30.8[c]	-	-
	30.7[d]	-	-
$Mg^{2+} + UO_2^{2+} + 3CO_3^{2-} \rightleftarrows MgUO_2(CO_3)_3^{2-}$	26.40[e]	-50.85[b]	0.09[e]
	26.2[c]	-	-
	25.8[d]	-	-0.02[d,*]
$UO_2^{2+} + SO_4^{2-} \rightleftarrows UO_2(SO_4)$	3.15	19.5	-
$UO_2^{2+} + 2SO_4^{2-} \rightleftarrows UO_2(SO_4)_2^{2-}$	4.14	35.1	-0.12
$UO_2^{2+} + 3SO_4^{2-} \rightleftarrows UO_2(SO_4)_3^{4-}$	3.02	-	-

a Shang and Reiller (2020); b Shang and Reiller (2021a); c Grenthe et al. (2020), Thermochimie 11a; d Thermochimie 10a,d; e Shang and Reiller (2021b); * error corrected from analogy of like-charged analysis in Thermochimie 10d.

Table S2. Equations of the principal axes of the ellipsoids for $CaUO_2(CO_3)_3^{2-}$, $Ca_2UO_2(CO_3)_3(aq)$, and $UO_2CO_3(aq)$ species, determined in $\log_{10}(a(Mg^{2+})^n\, a(Ca^{2+})^{(1-n)}/a(H^+)^2) - \log_{10}(a(Na^+)/a(H^+)) - \log_{10}(a(HCO_3^-)\, a(H^+))$ space.

	Principal semi-axes	First Principal Axis	Second Principal Axis	Third Principal Axis
$CaUO_2(CO_3)_3^{2-}$	a = 3.82799	x = 11.7723 – 0.748772 t	x = 11.7723 + 0.328566 t	x= 11.7723 – 0.575661 t
	b = 1.16547	y = –10.0765 + 0.295652 t	y = –10.0765 – 0.61175 t	y = –10.0765 – 0.733724 t
	c = 0.528364	z = 5.295 – 0.593238 t	z = 5.295 – 0.719587 t	z = 5.295 + 0.36092 t
$Ca_2UO_2(CO_3)_3(aq)$	a = 2.72568	x = 11.6464 – 0.776451 t	x = 11.6464 + 0.0511427 t	x = 11.6464 – 0.628099 t
	b = 0.892228	y = –9.65977 + 0.583603 t	y = –9.65977 – 0.317697 t	y = –9.65977 – 0.747313 t
	c = 0.300152	z = 4.83921 – 0.237765 t	z = 4.83921 – 0.946812 t	z = 4.83921 + 0.216829 t
$UO_2CO_3(aq)$	a = 1.81932	x = 8.77499 – 0.859795 t	x = 8.77499 – 0.493255 t	x = 8.77499 + 0.132107 t
	b = 0.662122	y = –9.8316 + 0.35214 t	y = –9.8316 – 0.385381 t	y = –9.8316 + 0.852923 t
	c = 0.423642	z = 2.8945 – 0.369797 t	z = 2.8945 + 0.77986 t	z = 2.8945 + 0.505044 t

References

Grenthe I., Gaona X., Plyasunov A.V., Rao L., Runde W.H., Grambow B., Koning R.J.M., Smith A.L., Moore E.E., 2020. Chemical Thermodynamics 14. Second Update on the Chemical Thermodynamics of Uranium, Neptunium, Plutonium, Americium and Technetium. Paris, France: OECD Nuclear Energy Agency Data Bank, Eds., OECD Publications, http://www.oecd-nea.org/jcms/pl_46643/second-update-of-u-np-pu-am-and-tc.

Shang C., Reiller P.E., 2020. Determination of formation constants and specific ion interaction coefficients for $Ca_nUO_2(CO_3)_3^{(4-2n)-}$ complexes in NaCl solution by time-resolved laser-induced luminescence spectroscopy. Dalton Trans. 49, 466-481. http://doi.org/10.1039/C9DT03543E.

Shang C., Reiller P.E., 2021a. Effect of temperature on the complexation of triscarbonatouranyl(VI) with calcium and magnesium in NaCl aqueous solution. Dalton Trans. 50, 17165-17180. http://doi.org/10.1039/D1DT03204F.

Shang C., Reiller P.E., 2021b. Thermodynamic constant of $MgUO_2(CO_3)_3^{2-}$ complex in $NaClO_4$ and NaCl media using time-resolved luminescence spectroscopy, and applications to different geochemical contexts. Dalton Trans. 50, 4363-4379. http://doi.org/10.1039/d0dt04124f.